Design and Synthesis of Inductorless Passive Cell Operating as Stop-Band Negative Group Delay Function

Mathieu Guerin, Yang Liu, Alexandre Douyere, George Chan, Fayu Wan,
Sebastien Lallechere, Wenceslas Rahajandraibe, Blaise Ravelo

Design and Synthesis of Inductorless Passive Cell Operating as Stop-Band Negative Group Delay Function

MATHIEU GUERIN[1], (Member, IEEE), **YANG LIU**[2], **ALEXANDRE DOUYÈRE**[3], (Member, IEEE),
GEORGE CHAN[4], (Senior Member, IEEE), **FAYU WAN**[5], (Member, IEEE),
SÉBASTIEN LALLÉCHÈRE[6], (Member, IEEE),
WENCESLAS RAHAJANDRAIBE[1], (Member, IEEE),
AND BLAISE RAVELO[5], (Member, IEEE)

[1]CNRS, University of Toulon, IM2NP UMR7334, Aix-Marseille University, 13013 Marseille, France
[2]Altran, 78140 Vélizy-Villacoublay, France
[3]Energy Laboratory, Network and Telecom Team, University of la Reunion, La Reunion Island, 97715 Saint-Denis, France
[4]ASM Pacific Technology Ltd., Hong Kong
[5]School of Electronic and Information Engineering, Nanjing University of Information Science and Technology, Nanjing 210044, China
[6]Institut Pascal, SIGMA, Université Clermont Auvergne, 63001 Clermont, France

Corresponding author: Yang Liu (liuyang2101@gmail.com)

ABSTRACT This paper develops an original circuit theory of unfamiliar stop-band (SB) negative group delay (NGD) topology. The proposed NGD topology is implemented without inductor component. The developed theory is established with passive cell constituted by RC-network based high-pass (HP) and low-pass (LP) NGD composite circuits. The analytical investigation of the SB-NGD circuit is introduced from the elaboration of voltage transfer function (VTF). The canonical form enabling to identify SB-NGD circuit is analytically expressed. The different SB-NGD characteristics as GD value, and, center and cut-off frequencies are innovatively formulated in function of the circuit resistor and capacitor components. The existence condition of SB-NGD function is also established. The inductorless SB-NGD topology is validated by a proof-of-concept (POC) circuit implemented by surface-mounted-device (SMD) component based printed circuit board (PCB). The measured VTF magnitude and group delay (GD) are extracted from the experimented S-parameters. A good agreement between the calculated, simulated and measured results is obtained. The SB-NGD behavior has measured center frequency of about 32 MHz. The lower- and upper-NGD cut-off frequencies are about 9.15 MHz and 98.3 MHz. The optimal NGD values at low and higher frequencies are -3.25 ns and -56 ps.

INDEX TERMS Circuit theory, negative group delay (NGD), stop-band (SB) NGD function, passive cell, inductorless topology.

I. INTRODUCTION

Since the invention of the integrated circuit, the design technology of modern electronic devices evolves spectacularly with the tremendous expansion of semiconductor industry. In spite of the technological progress, the modern electronic and communication systems still suffer from undesirable

effects as signal noise and delay [1], [2]. The delay effects are drastically limiting the performances of printed circuit boards (PCBs) because of the influence of electrical interconnects [3]. In opposite of the negative effect, somehow the group delay (GD) was exploited to design innovative RF and microwave circuits [4].

To deal against the delay effects, tentative solutions were proposed by using the negative group delay (NGD) function [5]–[8]. However, nowadays, compared to other classical

electronic functions, the NGD is still not familiar to most of design, fabrication, sell and research engineers. Therefore, more pedagogical research works need to be done to make the NGD engineering to be open to all electronic design engineers. For the best comprehension, let start the present study by a brief state of the art about the NGD electronic engineering.

The NGD function was initially experimented in the area of optical engineering [9], [10]. The initial experimentation was brilliantly carried out with negative group velocity (NGV) optical media. Hence, by inspiring to the negative refractive index (NRI) metamaterials [11], [12], the NGD function was uncommonly verified in the area of microwave engineering. But the results were less successful because the typical metamaterial based NGD circuits were implemented with periodical and cumbersome design structures. Consequently, the metamaterial NGD circuits were critically experimented with inherent losses. In addition, the unconventional NGD principles often lead electronic designers to ask curious questions notably about the NGD existence. To answer to such curious question, further research effort is needed to highlight the meaning of NGD function to non-specialist electronic design engineers. The simplest manner to theorize and classify the NGD function was introduced by considering the similarity with the filter behavior [13]. Different classes as low-pass (LP) [14]–[16], high-pass (HP) [17] and bandpass (BP) [18] NGD topologies were categorized. Last two decades, the challenging design of low-attenuation and compact BP NGD circuits attracted particularly the attention of some electronic design and research engineers [18]–[26]. Therefore, a huge diversity of fascinating BP-NGD topologies was reported [18]–[26]. For example, by using absorptive bandstop filter [20], a prescribed BP-NGD passive circuit was designed; in [21], [22], an active transversal-filter-based BP-NGD circuit was introduced. Some complex designs showing BP-NGD function with signal interference techniques [23] were also investigated. Then, last ten years, significant NGD research works were performed to develop a new family of BP-NGD distributed circuit based on microstrip transmission lines (TLs) [24]–[26]. Innovative design solutions of compact and low-attenuation BP-NGD circuits were proposed with transmission-type [24], self-matched [25] and defected plane structures [26].

Behind the significant interests on the BP-NGD microwave circuit design, we would like to highlight further about other different NGD topologies. With a wider research view on the NGD topological investigation, we are wondering about the designability of stop-band (SB) NGD novel circuit. The main purpose of the present paper is to develop a novel circuit theory of SB-NGD topology. The passive circuit is implemented by the cascade combination of HP-LP composite NGD cells. In other words, it is important to emphasize that the proposed SB-NGD topology does not use any inductor lumped component and any resonance network. This original NGD passive topology is implemented as inductorless circuit only constituted by resistive and capacitive network. In brief,

this research work introduces a remarkable contribution in the area of circuit and system engineering which is never being done before. The remarkable contributions are:

- An original theorization of SB-NGD inductorless circuit without use of resonant circuit,
- The analysis and characterization of SB-NGD circuit with the formulas of synthesis method,
- And the new design method of SB-NGD circuit based on inductorless topology.

The present paper is organized in three sections as follows:

- Section II introduces the SB-NGD passive topology under study. It is composed of HP- and LP-NGD composite cells. It acts as a first investigation of SB-NGD circuit theory constituted by inductorless topology.
- Section III is focused on the SB-NGD analytical characterization. The theory is established by developing a voltage transfer function (VTF) canonical form. The main SB-NGD characteristics are formulated in function of the constituting resistive and capacitive parameters.
- Section IV verifies the relevance of the SB-NGD theory of inductorless topology. A proof-of-concept (PoC) of LP-HP composite RC-network circuit is design and fabricated. The obtained validation results of the SB-NGD behavior will be discussed by comparison of calculation, simulation and measurement.
- Then, Section V is the final conclusion of the paper.

II. THEORY OF INDUCTORLESS SB-NGD TOPOLOGY

The present section describes the topological representation of the SB-NGD passive circuit under study. Then, the ideal specifications of the SB-NGD function and the associated characteristics are defined.

A. SB-NGD TOPOLOGY AND VTF EXPRESSION

The circuit representation of the SB-NGD topology is introduced in the present subsection. The innovative circuit constituted by the combination of RC-network based elementary HP- and LP-NGD composite cells will be studied. Then, the analytical VTF will be expressed in function of the constituting resistive and capacitive components.

1) TOPOLOGICAL DESCRIPTION

The present topological approach of SB-NGD circuit is based on the consideration of passive resistive and capacitive network. Fig. 1(a), Fig. 1(b) and Fig. 1(c) depict the circuit representation of LP-, HP- and SB-NGD passive circuit cells, respectively. We can emphasize that the SB- NGD topology depicted by Fig. 1(c) is also an HP-LP composite cell. It can be emphasized that the circuit behaves as an inductorless cell composed only by RC-network. The considered topology is constituted by:

- an LP-NGD passive cell presented by Fig. 1(a) with R_l-series and R_hC_h-series network
- and an HP-NGD passive cell shown by Fig. 1(b) with a series impedance of R_hC_h-parallel network and R_l resistance.
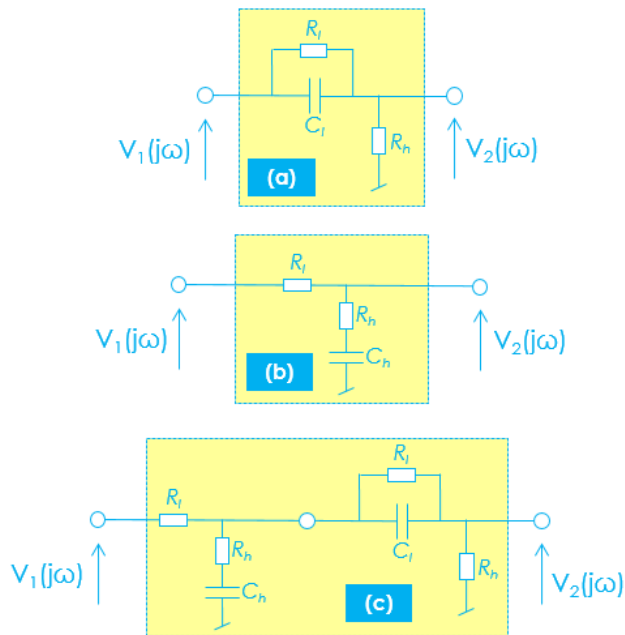
FIGURE 1. Topology of (a) LP-NGD cell, (b) HP-NGD cell and (c) SB-NGD cell.

To elaborate the VTF, the presented cells are assumed attacked by input voltage, V_1, and output voltage, V_2.

The following paragraph explores the VTF in function of the resistor and capacitor component parameters.

2) VTF EXPRESSION OF THE SB-NGD TOPOLOGY UNDER STUDY

Similar to the filter function analysis, the concrete implementation of the SB-NGD topology is here given through the VTF defined by:

$$T(s) = \frac{V_2(s)}{V_1(s)} \qquad (1)$$

by denoting with $s = j\omega$, and the angular frequency, ω, is the Laplace variable. After application of the Kirchhoff circuit law (KCL), the previous VTF can be rewritten:

$$T(s) = \frac{R_h(R_l C_l s + 1)(R_h C_h s + 1)}{\zeta_2 s^2 + \zeta_1 s + \zeta_0} \qquad (2)$$

with the denominator coefficients:

$$\zeta_2 = R_h C_h R_l C_l (R_l + 2R_h) \qquad (3)$$
$$\zeta_1 = C_h(R_l^2 + R_h^2) + R_l [R_l C_l + R_h(C_l + C_h)] \qquad (4)$$
$$\zeta_0 = 2R_l + R_h. \qquad (5)$$

The ideal specifications of the SB-NGD function knowing this VTF will be described in the following subsection.

B. IDEAL SPECIFICATIONS OF SB-NGD FUNCTION

At this stage, most of electronics engineer are wondering about the specification method of the unfamiliar SB-NGD

function. In the present subsection, the SB-NGD function diagram will be defined under the similar ways as the cases of LP-, HP- and bandpass (BP)-NGD ones.

1) GD DIAGRAM OF IDEAL SB-NGD FUNCTION

Fig. 2(a) and Fig. 2(b) represent the ideal GD diagrams illustrating the LP- and HP-NGD function responses, respectively.
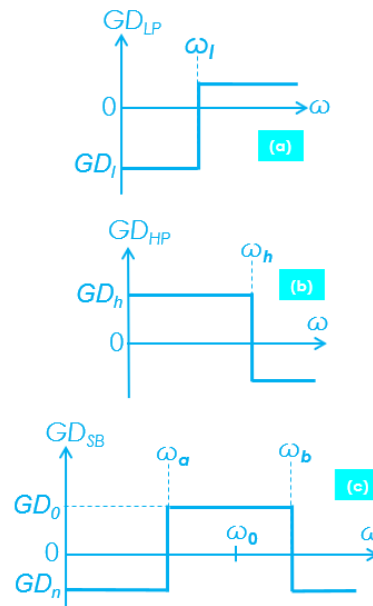

FIGURE 2. Ideal diagram responses: (a) LP-, (b) HP- and (c) SB-NGD functions.

The characterizations of these unfamiliar NGD functions can be described as follows:

- The GD response associated to the LP-NGD function is represented GD_{LP} as depicted by Fig. 2(a). This diagram is characterized by the pair (NGD value, NGD cut off angular frequency) or ($GD_l < 0$, ω_l).
- Then, the HP-NGD response shown by Fig. 2(b) is represented by GD_{HP}. This NGD function is characterized by the pair (NGD value, NGD cut off angular frequency) abbreviated by ($GD_h > 0$, ω_h).

The unfamiliar SB-NGD function response is represented by the diagram GD_{SB} shown by Fig. 2(c). The frequency response diagram is characterized by the cut-off angular frequencies, $\omega_a < \omega_b$. The associated NGD bandwidth (BW) is given by:

$$\Delta\omega = \omega_b - \omega_a. \qquad (6)$$

Then, the specific parameters of the negative and positive GD values can be denoted by $GD_0 > 0$ and $GD_n < 0$, respectively.

For more detailed analytical approach, the canonical form of VTF is explored in the subsection.

C. CANONICAL FORM AND ANALYTICAL EXPRESSION OF THE SB-NGD VTF

Similar to the BP-NGD case, the canonical form of SB-NGD function is elaborated in the present subsection. The analytical expression is defined by the second order polynomial formula:

$$T(s) = \frac{T_0(s^2 + \omega_n s + \omega_0^2)}{s^2 + \omega_d s + \omega_0^2}. \tag{7}$$

By identification with the VTF written in formula (2), the parameters of this canonical form can be written as follows:

$$T_0 = \frac{R_h}{R_h + 2R_l} \tag{8}$$

$$\omega_n = \frac{R_h C_h + R_l C_l}{R_h C_h R_l C_l} \tag{9}$$

$$\omega_d = \frac{R_l^2(C_l + C_h) + R_h^2 C_h + R_l R_h(C_l + 3C_h)}{R_h C_h R_l C_l(2R_l + R_h)} \tag{10}$$

$$\omega_0 = \frac{1}{\sqrt{R_h C_h R_l C_l}}. \tag{11}$$

Knowing this canonical form, we can develop the SB-NGD analysis of the circuit presented in Fig. 1(c). The following section present the analytical result.

III. SB-NGD ANALYSIS OF INDUCTORLESS SB-NGD CELL UNDER STUDY

The present section introduces the analytical specifications of SB-NGD function in function of the resistive and capacitive parameters of the circuit topology. The SB-NGD main characteristics will be exploited.

A. MAGNITUDE ANF GD OF THE SB-NGD VTF

The corresponding magnitude by means of the VTF canonical form proposed in equation (7). As matter of fact, we have the magnitude of the canonical form VTF expressed as:

$$T(\omega) = \frac{T_0\sqrt{(\omega_0^2 - \omega^2)^2 + \omega_n^2 \omega^2}}{\sqrt{(\omega_0^2 - \omega^2)^2 + \omega_d^2 \omega^2}}. \tag{12}$$

The associated VTF phase is given by:

$$\varphi(\omega) = \arctan\left(\frac{\omega_n \omega}{\omega_0^2 - \omega^2}\right) - \arctan\left(\frac{\omega_d \omega}{\omega_0^2 - \omega^2}\right). \tag{13}$$

The analytical expression of GD becomes:

$$GD(\omega)$$
$$= \frac{(\omega_d - \omega_n)(\omega^2 + \omega_0^2)\left[\omega^4 - (\omega_n \omega_d + 2\omega_0^2)\omega^2 + \omega_0^4\right]}{\left[\omega^4 + (\omega_n^2 - 2\omega_0^2)\omega^2 + \omega_0^4\right]\left[\omega^4 + (\omega_p^2 - 2\omega_0^2)\omega^2 + \omega_0^4\right]} \tag{14}$$

These analytical expressions will serve to the SB-NGD characterization developed in the following subsection.

B. SB-NGD ANALYTICAL CHARACTERIZATION

The SB-NGD characterization consists in the determination of the specific values of GDs, frequencies and VTF magnitudes. The specific frequencies for the present theoretical approach are the initial and very low frequencies (VLF) where $\omega \approx 0$ and resonant (ω_0) ones. The following paragraphs present the analytical expressions of GD and VTF magnitudes as such frequencies.

1) CHARACTHERIZATION AT VLF

We can demonstrate from the magnitude given in equation (12) that at very low frequencies, we have:

$$T(\omega \approx 0) = T_0. \tag{15}$$

Then, it can be established that the GD given in equation (14) is transformed as:

$$GD(\omega \approx 0) = \frac{\omega_d - \omega_n}{\omega_0^2}. \tag{16}$$

It interesting to underline that this GD is negative when:

$$\omega_d \leq \omega_n. \tag{17}$$

By taking into account relations (8) and (9), the previous condition implies the following inequality between the resistive and capacitive components of our SB-NGD circuit:

$$\begin{bmatrix} R_l^2(C_l + C_h) + R_h^2 C_h \\ + R_l R_h(C_l + 3C_h) \end{bmatrix} \leq (2R_l + R_h)(R_h C_h + R_l C_l). \tag{18}$$

This inequality constitutes an initial existence condition of SB-NGD function.

2) ANALYSIS AT THE CENTER FREQUENCY

The SB-NGD analysis is also explored from the VTF canonical form. It consists mainly in the determination of the NGD cut-off frequencies which are the root of equation:

$$GD(\omega) = 0 \tag{19}$$

As illustrated by Fig. 2(c), the SB-NGD cut-off frequencies separate the NGD lower and upper frequency bands. By considering the GD given by equation (14), we can demonstrate that the associated lower and upper cut-off frequencies formulated as, respectively:

$$\omega_a = \sqrt{\omega_0^2 + \frac{\omega_n \omega_d - \sqrt{\omega_n \omega_d(4\omega_0^2 + \omega_n \omega_d)}}{2}} \tag{20}$$

$$\omega_b = \sqrt{\omega_0^2 + \frac{\omega_n \omega_d + \sqrt{\omega_n \omega_d(4\omega_0^2 + \omega_n \omega_d)}}{2}}. \tag{21}$$

Moreover, at angular frequency, $\omega = \omega_0$, the VTF magnitude of the HP-LP cell expressed in equation (12) is simplified as:

$$T(\omega_0) = \frac{T_1 \omega_n}{\omega_d}. \tag{22}$$

Thus, the GD expressed in equation (14) becomes:

$$GD(\omega_0) = \frac{2(\omega_n - \omega_d)}{\omega_n \omega_d}. \tag{23}$$

Knowing these expressions, we can establish the general conditions of SB-NGD function existence.

3) GENERAL CONDITION OF SB-NGD FUNCTION EXISTENCE

Following the ideal specification introduced by the diagram of Fig. 2(c), the GD response can be assumed as SB-NGD function if the following inequalities are satisfied:

$$\begin{cases} GD(\omega \approx 0) < 0 \\ GD(\omega_0) > 0. \end{cases} \tag{24}$$

After simplification, both inequalities lead to the following condition:

$$C_h(R_l + R_h) \le R_l C_l. \tag{25}$$

This later condition will serve to choose the resistor and capacitor components for designing a SB-NGD circuit prototype.

The next subsection will be devoted to the prescription of LP-HP circuit parameters with respect to the desired SB NGD specifications.

C. SYNTHESIS EQUATIONS OF THE RESISTORS AND CAPACITORS CONSTITUTING THE SB-NGD CELL

The design of the HP-LP NGD composite cell can be performed with respect to the targeted SB-NGD specifications. For example, given the attenuation A, we can solve the equation:

$$T(\omega_0) = A. \tag{26}$$

The SB-NGD cell can be synthesized by solving the derived equation:

$$T(\omega_0) = T_0 \left[1 + \frac{GD_0 \Delta\omega(\xi + GD_0 \Delta\omega)}{8} \right] \tag{27}$$

with:

$$\xi = \sqrt{16 + (GD_0 \Delta\omega)^2}. \tag{28}$$

The other equation is based on the given GD value:

$$GD(\omega_0) = GD_0 > 0 \tag{29}$$

at the angular frequency, ω_0, and bandwidth, $\Delta\omega$. We can demonstrate by inverting equations (26) and (29) that the SB NGD canonical TF parameters can be determined by the relations:

$$\omega_n = \frac{\Delta\omega(\xi + GD_0 \Delta\omega)}{4} \tag{30}$$

$$\omega_d = \frac{\Delta\omega(\xi - GD_0 \Delta\omega)}{4}. \tag{31}$$

By fixing, R_h, the main unknowns of the inductorless SB NGD circuit synthesis are R_l, C_l, and C_h. By taking into account equation (9) and equation (10), we have:

$$R_l = \frac{R_h [8 - 8A + GD_0 \Delta\omega(\xi + GD_0 \Delta\omega)]}{16 T_0} \tag{32}$$

$$C_l = \frac{\Delta\omega T_0 \left[\xi(1 - T_0^2) + GD_0 \Delta\omega(1 + 8T_0 - T_0^2) \right]}{2 R_h \omega_0^2 (3T_0 + 1)(T_0 - 1)^2} \tag{33}$$

$$C_h = \frac{\Delta\omega T_0 \left[\xi(T_0 - 1) + GD_0 \Delta\omega(3 + T_0) \right]}{2 R_h \omega_0^2 (3T_0 + 1)(T_0 - 1)^2}. \tag{34}$$

The existence of these component values depends on conditions ($R_l > 0$, $C_l > 0$, $C_h > 0$). Therefore, the synthesis must satisfy the conditions:

$$A < 1 + \frac{GD_0 \Delta\omega(\xi + GD_0 \Delta\omega)}{8} \tag{35}$$

$$T_0^2 - \frac{8GD_0 \Delta\omega}{\xi + GD_0 \Delta\omega} T_0 - \frac{\xi + GD_0 \Delta\omega}{\xi + GD_0 \Delta\omega} < 0 \tag{36}$$

$$T_0 > \frac{\xi - 3GD_0 \Delta\omega}{\xi + GD_0 \Delta\omega}. \tag{37}$$

To verify the design feasibility of the SB NGD topology, a PoC investigated by simulation and measurement will be depicted and studied in the following section.

IV. CALCULATED, SIMULATED AND EXPERIMENTED SB-NGD RESULTS

The present section focuses on the feasibility study of the LP-HP composite NGD circuit design. The practical study will be developed with an RC-network prototype. After the PoC description, the calculated, simulated and measured results are discussed. Then, sensitivity analyses (SAs) with respect to +/−5% relative variation of the inductorless circuit constituting elements are presented.

A. DESCRIPTION OF THE INDUCTORLESS SB-NGD POC PROTOTYPES

The prototype of LP-HP composite NGD circuit was implemented on Cu-metalized FR4 dielectric substrate in hybrid technology with surface mounted device (SMD) of resistor and capacitor elements. The components are provided by the manufacturer with +/−5% relative tolerances. The proof-of-concept circuit was design with synthesis equation (32), equation (33) and equation (34). The ideal values of components, R_l, C_l and C_h were determined by these formulas, respectively. The NGD circuit prototype introduced was designed and fabricated. Fig. 3(a) shows the schematic of the designed circuit in the schematic environment of the electronic and RF/microwave circuit simulator ADS® from Keysight Technologies. The fabricated prototype is shown in Fig. 3(b).

The electrical parameters of this prototype are indicated in Table 1.

B. MEASUREMENT TECHNIQUE OF THE SB-NGD CIRCUIT

The validation of the considered SB-NGD circuit is performed by means of S-parameter measurement technique.
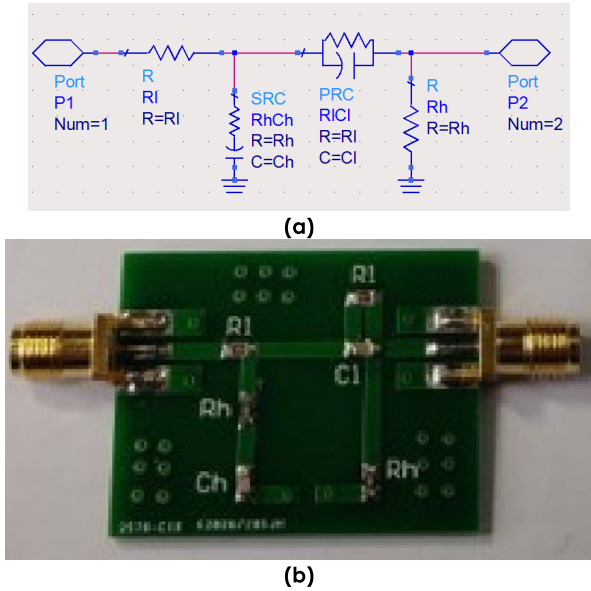
(a)

(b)

FIGURE 3. (a) Schematic and (b) photograph of the SB-NGD circuit prototype (size 28 mm × 21 mm).

TABLE 1. Parameters of the LP-HP Composite NGD Prototype.

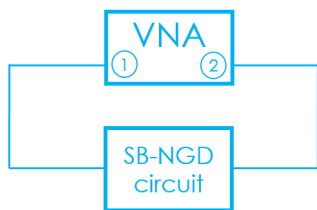| Function	Designation	Parameter	Ideal value	Nominal value
Desired specification	Center frequency	f_0	30 MHz	
	NGD value	GD_0	1 ns	
	Attenuation	A	-7 dB	
LP-HP composite NGD circuit parameters	Resistor	R_h	40 Ω	39 Ω
		R_l	38.02 Ω	39 Ω
	Capacitor	C_l	364.8 pF	360 pF
		C_h	44.56 pF	51 pF

FIGURE 4. Illustrative diagram of the SB-NGD circuit measurement.

The following paragraph describes the performed technique and the results post-processing in order to extract the VTF.

1) DESCRIPTION OF THE SB-NGD CIRCUIT EXPERIMENTAL SETUP

Fig. 4 shows the illustrative diagram of the measurement technique of the SB-NGD circuit under study. The measurement is based on the consideration of two-port Vector Network Analyzer (VNA) connected to the SB-NGD circuit which is assumed as the device under test.

Fig. 5 presents the realized photograph of the experimental setup including the fabricated SB-NGD circuit prototype.
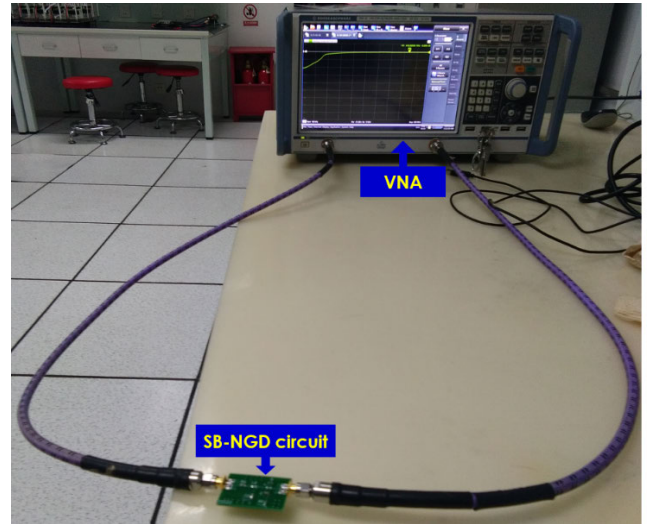

FIGURE 5. Experimental setup of the LP-HP composite SB-NGD circuit prototype.

The experimental test was carried out by using a VNA with reference Rohde & Schwarz ZNB 20, within the frequency band 100 kHz to 20 GHz.

2) TRANSFORM EQUATION TO DETERMINE THE MEASURED VTF FROM THE S-PARAMETERS

The measured data were recorded in touchstone format. The data are represented as f-frequency dependent 2-D S-matrix. In other words, the raw data are two-dimensional matrix of complex numbers represented by:

$$[S(jf)] = \begin{bmatrix} S_{11}(jf) & S_{12}(jf) \\ S_{21}(jf) & S_{22}(jf) \end{bmatrix}. \qquad (38)$$

The measured VTF of the tested LP-HP composite NGD circuit is extracted from S-parameters. The S-parameter to VTF transform is represented by the following relation:

$$T(jf) = \frac{S_{21}(jf)}{[1 + S_{11}(jf)][1 - S_{22}(jf)] + S_{12}(jf)S_{21}(jf)}. \qquad (39)$$

The obtained validation results of the SB-NGD circuit from this test will be presented in the following paragraph.

3) MEASURED S-PARAMETERS OF THE SB-NGD CIRCUIT

The S-parameter measurement was made in the frequency band from 1 MHz to 200 MHz. Fig. 6 plots the magnitudes of measured data. In top, we have reflection coefficient, S_{11} which decreased from about −10 dB to −25 dB. In the medium, the transmission coefficient represented by $S_{12} = S_{21}$ is plotted.

This graph presents concave shape with a maximum value of about −9.43 dB at about 29 MHz. Thus, the bottom plot is the output reflection coefficient presented by S_{22}. It increases with the frequency from about −12 dB to −6 dB. By using the S-parameters to VTF transform expressed by equation (39), the measured VTF was determined. The following
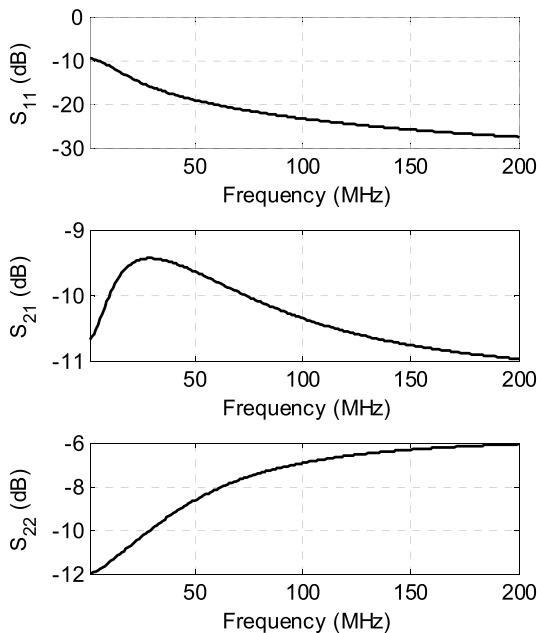
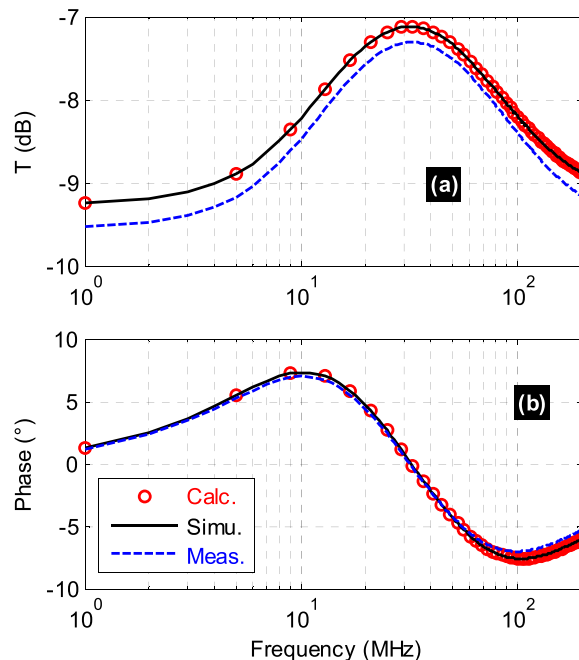**FIGURE 6.** Measured S-parameters of the SB-NGD circuit.

FIGURE 7. Comparisons of calculated, simulated, and measured VTF (a) magnitudes and (b) phases of SB-NGD circuit prototype.

FIGURE 8. Semi-logarithmic plots of calculated, simulated, and measured VTF (a) magnitudes and (b) phases of SB-NGD circuit prototype.
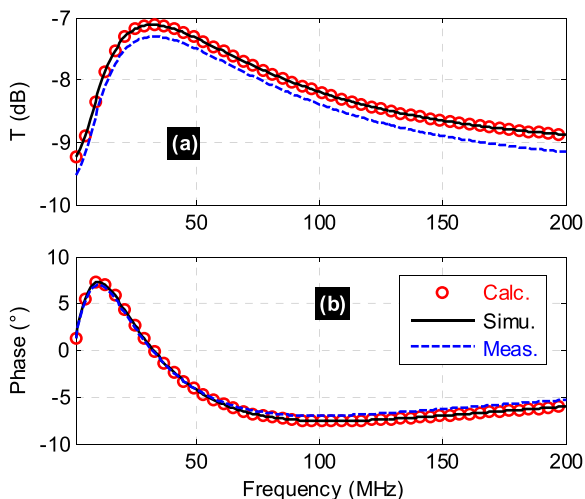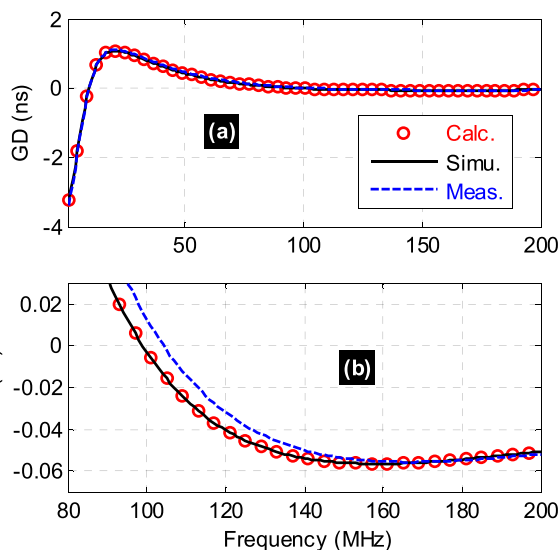

FIGURE 9. Comparisons of calculated, simulated, and measured VTF GDs of the SB-NGD circuit prototype in (a) wide and (b) narrow band.

subsections describe the comparative and SA results of magnitudes and GDs.

C. DISCUSSION ON THE SB-NGD VALIDATION RESULTS

The experimental validation of the SB-NGD function exhibited by the LP-HP composite NGD topology under study is proved by analytically calculated ("Calc."), simulated ("Simu.") with ADS®, and measured ("Meas.") results. The calculated results were obtained with a program developed in MATLAB® using VTF magnitude given by equation (15) and GD written by equation (17) of the tested circuits. The calculated, simulated, and measured VTF magnitudes and phases of the LP-HP composite NGD prototype

are plotted in Figs. 7 and the corresponding semilogarithmic plots shown by Figs. 8. We can emphasize that the three different sets of data present a very good agreement. Moreover, the results displayed in Figs. 9 confirm the SB-NGD function generated by the LP-HP composite circuit. The corresponding semi-logarithmic plots of GD are shown by Figs. 10.

The frequency band of the LP-NGD response delimited to $f_a = 9.15$ MHz, given in equation (23), can be understood with the wideband plot of Fig. 9(a). The measured NGD is around to -3.25 ns. The upper NGD frequency band starts
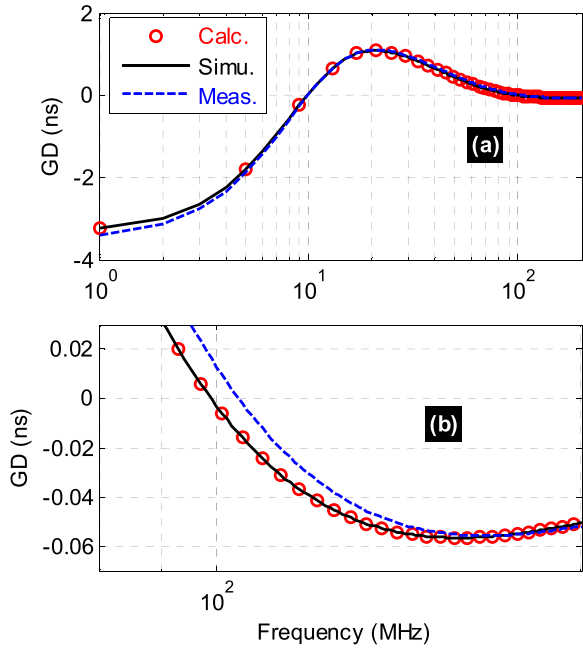
FIGURE 10. Semi-logarithmic plots of calculated, simulated, and measured VTF GDs of the SB-NGD circuit prototype in (a) wide and (b) narrow band.

TABLE 2. Comparison of Calculated, Simulated and Measured SB-NGD Specifications.

Approach	f_o	$GD(f_o)$	BW	$T(f_o)$
Calculated	32.01 MHz	0.88 ns	89.1 MHz	-7.12 dB
Simulated	32 MHz	0.87 ns	89.01 MHz	-7.11 dB
Measured	32 MHz	0.89	83.6 MHz	-7.3

from $f_b = 98.3$ MHz, defined in equation (24). The optimal NGD value in the higher frequencies is -56 ps. Table 2 indicates the comparison of SB-NGD specifications with measured center frequency of approximately $f_0 = 32$ MHz. The slight differences between the calculated and measured magnitudes of about 0.15 dB is due to the relative tolerances of the components.

We can underline from Fig. 9(a) that the GD is flatter in lower SB frequency band than in the upper one. This behavior of NGD response flatness aspect can be analytically explained by the polynomial analytical model of the SB-NGD GD expressed in equation (17). In fact, if the frequency increases that GD trends to the asymptotic value. However, at very low frequency, we have the LP-NGD aspect which presents a significant variation from very low frequency to the lower cut-off frequency. The flatness of lower SB-NGD band can be improved by designing several SB-NGD cells.

To illustrate this effect, sensitivity analyses were performed with results discussed in the following subsections.

D. SA WITH RESPECT TO R_h, R_l, C_h AND C_l
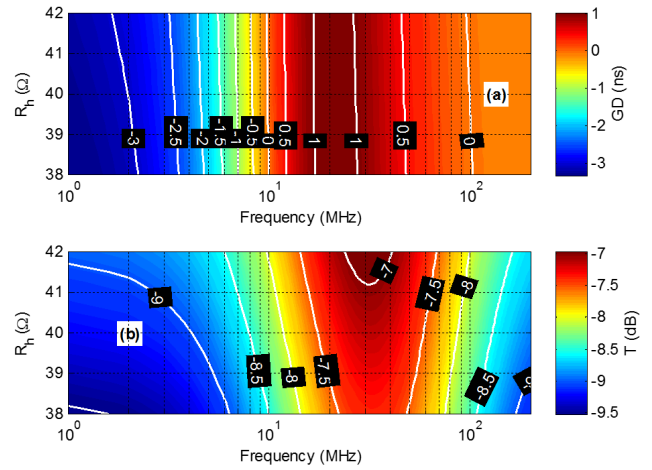The SAs of the LP-HP composite NGD circuit were carried out with MATLAB® calculations of VTF proposed in

FIGURE 11. Mappings of LP-HP NGD composite circuit (a) GD and (b) VTF magnitudes with respect to (R_h, f).
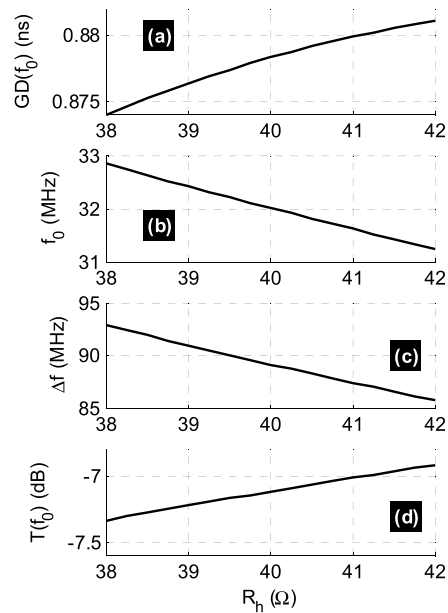

FIGURE 12. (a) GD at center frequency, (b) f_0, (c) bandwidth and (d) VTF magnitudes versus R_h.

equation (15). The SA computations were performed by linearly varying the four constituting components with relative variation of about $+/-5\%$ around the calculated ideal values introduced in Table 1. The following paragraphs present the obtained results with respect to the pair-couples (R_h, f), (R_l, f), (C_h, f) and (C_l, f), respectively.

1) INFLUENCE OF R_h
Fig. 11(a) introduces the obtained mapping of GD with respect to the couple (R_h, f). As the NGD behavior at higher frequencies is less significant than at lower frequencies, the mappings are plotted in semi-logarithmic scale. It can be underlined that the GD is negative at lower and higher frequencies as expected for the SB-NGD behavior.
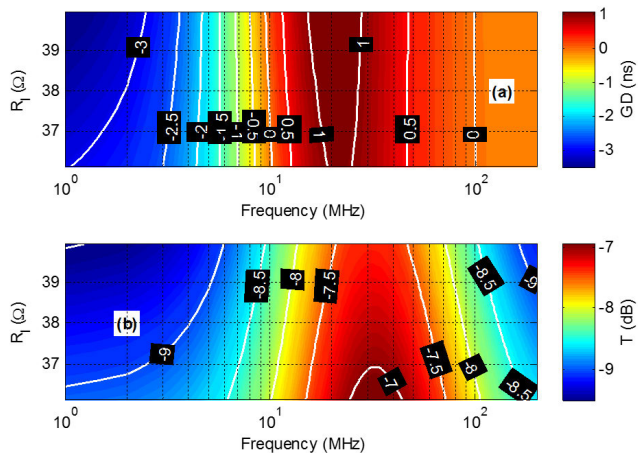
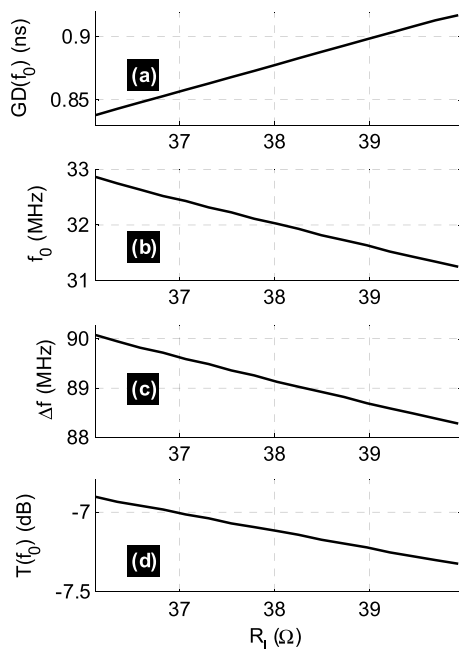**FIGURE 13.** Mappings of LP-HP NGD composite circuit (a) GD and (b) VTF magnitudes with respect to (R_l, f).

FIGURE 14. (a) GD at center frequency, (b) f_0, (c) bandwidth and (d) VTF magnitudes versus R_l.

FIGURE 15. Mappings of LP-HP NGD composite circuit (a) GD and (b) VTF magnitudes with respect to (C_h, f).

FIGURE 16. (a) GD at center frequency, (b) f_0, (c) bandwidth and (d) VTF magnitudes versus C_h.

It can be understood from Figs. 12 that the SB NGD bandwidths vary inversely proportional to R_h. Fig. 11(b) shows the mapping of the VTF magnitude from the SA of resistor R_h.

2) INFLUENCE OF R_l

Fig. 13(a) shows the mapping of GD with respect to the couple (R_l, f). Fig. 13(b) represent the associated magnitude mapping. Both figures are plotted in semi-logarithmic scale. As seen in Figs. 14, the SB NGD bandwidths vary proportionally to R_l. In this case, we can see again the SBNGD behavior is conserved despite the variation of the resistor element.

3) INFLUENCE OF C_h

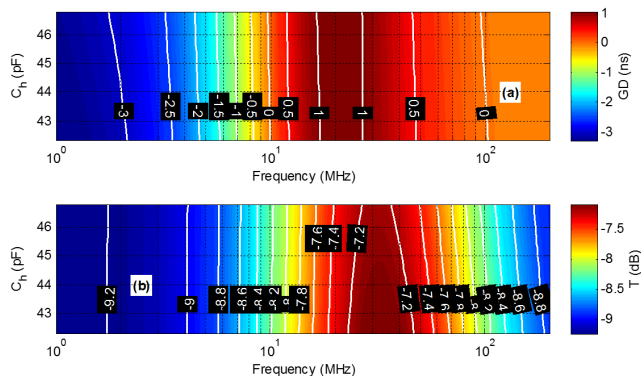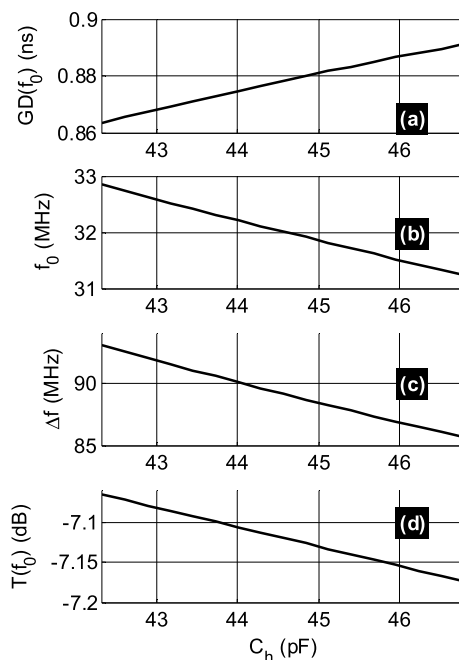Figs. 15(a) depicts the variation of the GD plotted in semi-logarithmic scale with respect to the couple (C_h, f).

Once again, the GD is clearly negative at very low and higher frequencies. This confirms the SB-NGD behavior signature.

Fig. 15(b) reports the associated magnitude. As depicted by Figs. 16, the SB NGD bandwidths vary inversely proportional to C_h and it is very interesting to emphasize that the magnitude at the center frequency is not sensitive to the capacitor variation.

4) INFLUENCE OF C_l

Figs. 17(a) represents the 2-D mapping of the GD plotted in semi-logarithmic scale with respect to the couple (C_j, f). Fig. 17(b) reports the associated magnitude. Once again, the GD is clearly negative at very low and higher frequencies. It can be pointed out from Figs. 18 that the SB-NGD bandwidths vary proportionally to C_l. This result confirms the SB-NGD behavior signature.

TABLE 3. Minimal and Maximal Parameters from SAs.

SA parameters		Δf (MHz)	f_0 (MHz)	$GD(f_0)$ (ns)	$T(f_0)$
R_{hmin}	38 Ω	85.74	31.24	0.87	0.430
R_{lmin}	36.12 Ω	88.27	31.24	0.84	0.430
C_{hmin}	42.33 pF	85.64	31.24	0.86	0.438
C_{lmin}	346.6 pF	88.38	31.24	0.85	0.438
R_{hmax}	42 Ω	92.86	32.84	0.88	0.451
R_{lmax}	39.92 Ω	90.10	32.84	0.92	0.451
C_{hmax}	46.79 pF	92.97	32.84	0.89	0.443
C_{lmax}	383 pF	89.99	32.84	0.91	0.443

TABLE 4. Comparison OF NGD Circuits Design.

References	Type of NGD function	Passive (P)/active (A)	With/without inductor lumped component
[13]		(A)	With
[14]	LP-NGD	(P)	With
[28]		(A)	Without
[29]		(A)	Without
[17] (*)	HP-NGD	(P)	Without
[30]		(P)	Both with and without
[13]		(A)	With
[18]		(P)	Without
[31]		(A)	With
[32]	BP-NGD	(A)	With
[33]		(A)	With
[34] (*)		(P)	With
[35]		(A)	With
[30]	SB-NGD	(P)	With
This work		(P)	Without

(*) The NGD study is based on equivalent impedance but not VTF

### 5) INFLUENCE ON SB-NGD SPECIFICATIONS

It can be deduced from the previous sensitivity analyses that the SB-NGD characteristics are slightly influenced by the resistive and capacitive component relative variations. Nevertheless, the range of GD value, center frequency, NGD cut-off frequencies and VTF magnitude needs to be assessed. The minimal and maximal values associated the SB NGD specifications in the range of SA values are summarized in Table 3.

### E. COMPARATIVE STUDY BETWEEN DIFFERENT TYPES OF NGD CIRCUIT

Despite the previous validation study, we may wonder about the original NGD specification of the SB-NGD circuit under study. To avoid this ambiguity, a comparative study between different lumped element based different types of NGD circuits available in the literature [13]–[17], [28]–[35] is drawn in the present subsection.

The performed comparative study can be summarized by Table 4.

The study is essentially focused on the types of NGD function, passive or active circuit design and the presence of inductor lumped element. We can report from this state of the art that:
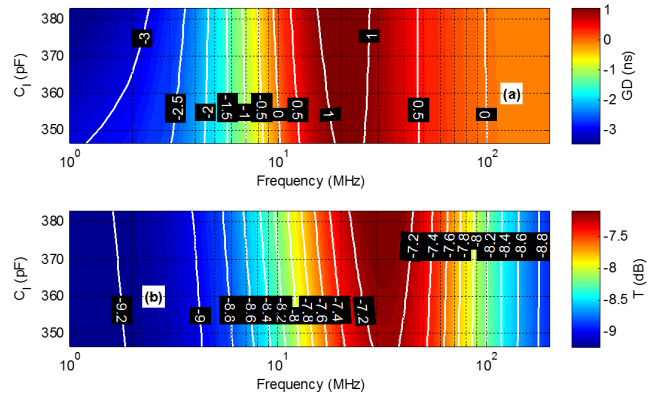
FIGURE 17. Mappings of LP-HP NGD composite circuit (a) GD and (b) VTF magnitudes with respect to (C_l, f).
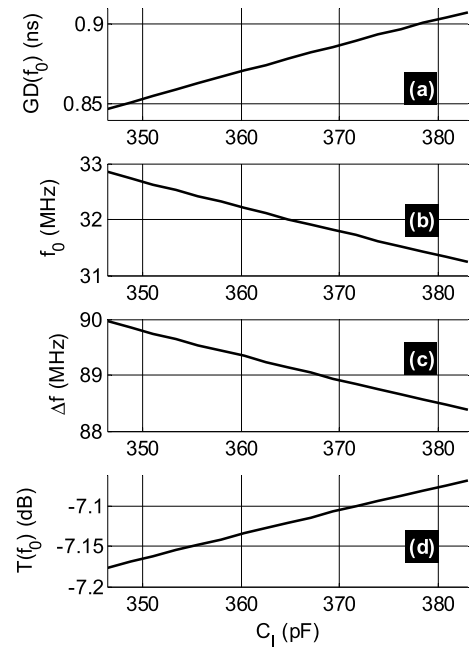
FIGURE 18. (a) GD at center frequency, (b) f_0, (c) bandwidth and (d) VTF magnitudes versus C_l.

- The existing LP-NGD circuits [13], [14], [28], [29] were designed and implemented with both passive and active circuits and also the possibility with and without inductor.
- The available design of few HP-NGD circuits [17], [30] are implemented as passive circuit.
- The most developed design of NGD circuits [13], [17], [31]–[35] are presenting BP-NGD type. In the summary table, it can be pointed out that the BP-NGD devices are designed active and passive lumped R, L and C component-based circuits.
- Because of the difficult counter intuitive interpretation, very few studies were made on the SB-NGD circuit [30]. The proposed innovative SB-NGD circuit is presenting an advantage in terms of design simplicity and also the

integrability because of the inductorless aspect. It is easier to control the flatness with RC-based network compared to RLC one. However, it is easier to control the maximal NGD absolute value with RLC-network based SB-NGD circuit.

V. CONCLUSION

Progressive research works on the NGD circuit design [9]–[23] were performed in the two-last decade. But the NGD design engineering is still unfamiliar to most of electronic engineers. To deal with this unsuccess, a classification of NGD circuit topologies consisted of LP-, HP- and BP-NGD function was initiated [12]. But so far, very less study is available on the SB-NGD circuit design.

An innovative circuit theory of SB-NGD topology is studied. The SB-NGD circuit constituted by HP-NGD NGD composite cell. The proposed SB-NGD topology operate only with RC-network. The passive circuit topology under study does not operate with resonant or LC-network and it operates without inductor lumped element. The SB-NGD transfer function canonical form is established. The synthesis equations allowing to determine the constituting RC-network parameters in function of the desired SB-NGD specifications are established. The performance of SB-NGD can be assessed with:

- The absolute value of NGD in the first and the second frequency bands,
- The bigger value of lower cut-off frequency f_a can be very useful in terms of applications,
- The GD flatness is very important between 0 Hz and the half of f_a,
- The SB-NGD circuit performance can be assessed with the flatness of GD in the expected operation frequency band,

The SB-NGD theory effectiveness is validated by experiments with an inductorless circuit PoC. The obtained results confirm the validity of the SB-NGD inductorless topology. As expected, a very good agreement between the calculation, simulation and measurement results is obtained and discussed. Further SAs were performed to highlight how each resistive and capacitive element affect the SB-NGD characteristics.

It is noteworthy that based on the best knowledge of the authors, there is no prototyping and validation study of SB-NGD circuit available in the literature. Nevertheless, we can state that the particular advantages of the developed SB NGD circuit design are:

- The SB-NGD circuit design simplicity with simple lumped components.
- The present study confirms the possibility of inductorless SB-NGD design. In fact, this point enables to envisage a potential miniaturization of SB-NGD circuit and also the possibility to operate at several tens gigahertz.
- Based on the previous advantage, the SB-NGD circuit is expected to be exploited for the innovative design of RF and microwave functions in the future.

REFERENCES

[1] S.-S. Myoung, B.-S. Kwon, Y.-H. Kim, and J.-G. Yook, "Effect of group delay in RF BPF on impulse radio systems," *IEICE Trans. Commun.*, vol. 90, no. 12, pp. 3514–3522, 2007.

[2] G. Groenewold, "Noise and group delay in active filters," *IEEE Trans. Circuits Syst. I, Reg. Papers*, vol. 54, no. 7, pp. 1471–1480, Jul. 2007.

[3] M. E. Hwang, S. O. Jung, and K. Roy, "Slope interconnect effort: Gate-interconnect interdependent delay modeling for early CMOS circuit simulation," *IEEE Trans. Circuits Syst. I, Reg. Papers*, vol. 56, no. 7, pp. 1428–1441, Jul. 2009.

[4] B. Nikfal, S. Gupta, and C. Caloz, "Increased group-delay slope loop system for enhanced-resolution analog signal processing," *IEEE Trans. Microw. Theory Techn.*, vol. 59, no. 6, pp. 1622–1628, Jun. 2011.

[5] K.-P. Ahn, R. Ishikawa, and K. Honjo, "Group delay equalized UWB InGaP/GaAs HBT MMIC amplifier using negative group delay circuits," *IEEE Trans. Microw. Theory Techn.*, vol. 57, no. 9, pp. 2139–2147, Sep. 2009.

[6] B. Ravelo, S. Lalléchére, A. Thakur, A. Saini, and P. Thakur, "Theory and circuit modeling of baseband and modulated signal delay compensations with low-and band-pass NGD effects," *Int. J. Electron. Commun.*, vol. 70, no. 9, Sep. 2016, pp. 1122–1127.

[7] T. Shao, Z. Wang, S. Fang, H. Liu, and Z. N. Chen, "A full-passband linear-phase band-pass filter equalized with negative group delay circuits," *IEEE Access*, vol. 8, pp. 43336–43343, 2020.

[8] J.-K. Xiao, Q.-F. Wang, and J.-G. Ma, "Negative group delay circuits and applications: Feedforward amplifiers, phased-array antennas, constant phase shifters, non-foster elements, interconnection equalization, and power dividers," *IEEE Microw. Mag.*, vol. 22, no. 2, pp. 16–32, Feb. 2021.

[9] B. Ségard and B. Macke, "Observation of negative velocity pulse propagation," *Phys. Lett. A*, vol. 109, pp. 213–216, May 1985.

[10] B. Macke and B. Ségard, "Propagation of light-pulses at a negative group-velocity," *Eur. Phys. J. D*, vol. 23, no. 1, pp. 125–141, Apr. 2003.

[11] G. V. Eleftheriades, O. Siddiqui, and A. K. Iyer, "Transmission line for negative refractive index media and associated implementations without excess resonators," *IEEE Microw. Wireless Compon. Lett.*, vol. 13, no. 2, pp. 51–53, Feb. 2003.

[12] O. F. Siddiqui, M. Mojahedi, and G. V. Eleftheriades, "Periodically loaded transmission line with effective negative refractive index and negative group velocity," *IEEE Trans. Antennas Propag.*, vol. 51, no. 10, pp. 2619–2625, Oct. 2003.

[13] B. Ravelo, "Similitude between the NGD function and filter gain behaviours," *Int. J. Circuit Theory Appl.*, vol. 42, no. 10, pp. 1016–1032, Oct. 2014.

[14] B. Ravelo, "First-order low-pass negative group delay passive topology," *Electron. Lett.*, vol. 52, no. 2, pp. 124–126, Jan. 2016.

[15] F. Wan, N. Li, B. Ravelo, J. Ge, and B. Li, "Time-domain experimentation of NGD active RC-network cell," *IEEE Trans. Circuits Syst. II, Exp. Briefs*, vol. 66, no. 4, pp. 562–566, Apr. 2019.

[16] F. Wan, T. Gu, B. Ravelo, B. Li, J. Q. Cheng Yuan, and J. Ge, "Negative group delay theory of a four-port RC-network feedback operational amplifier," *IEEE Access*, vol. 7, pp. 75708–75720, 2019.

[17] B. Ravelo, "High-pass negative group delay RC-network impedance," *IEEE Trans. Circuits Syst. II, Exp. Briefs*, vol. 64, no. 9, pp. 1052–1056, Sep. 2017.

[18] B. Ravelo, S. Ngoho, G. Fontgalland, L. Rajaoarisoa, W. Rahajandraibe, R. Vauché, Z. Xu, F. Wan, J. Ge, and S. Lalléchère, "Original theory of NGD low pass-high pass composite function for designing inductorless BP NGD lumped circuit," *IEEE Access*, vol. 8, pp. 192951–192964, 2020.

[19] C.-T. M. Wu and T. Itoh, "Maximally flat negative group-delay circuit: A microwave transversal filter approach," *IEEE Trans. Microw. Theory Techn.*, vol. 62, no. 6, pp. 1330–1342, Jun. 2014.

[20] L.-F. Qiu, L.-S. Wu, W.-Y. Yin, and J.-F. Mao, "Absorptive bandstop filter with prescribed negative group delay and bandwidth," *IEEE Microw. Wireless Compon. Lett.*, vol. 27, no. 7, pp. 639–641, Jul. 2017.

[21] H. Mirzaei and G. V. Eleftheriades, "Realizing non-Foster reactive elements using negative-group-delay networks," *IEEE Trans. Microw. Theory Techn.*, vol. 61, no. 12, pp. 4322–4332, Dec. 2013.

[22] T. Zhang, R. Xu, and C.-T. M. Wu, "Unconditionally stable non-foster element using active transversal-filter-based negative group delay circuit," *IEEE Microw. Wireless Compon. Lett.*, vol. 27, no. 10, pp. 921–923, Oct. 2017.

[23] Z. Wang, Y. Cao, T. Shao, S. Fang, and Y. Liu, "A negative group delay microwave circuit based on signal interference techniques," *IEEE Microw. Wireless Compon. Lett.*, vol. 28, no. 4, pp. 290–292, Apr. 2018.

[24] G. Liu and J. Xu, "Compact transmission-type negative group delay circuit with low attenuation," *Electron. Lett.*, vol. 53, no. 7, pp. 476–478, Mar. 2017.

[25] T. Shao, Z. Wang, S. Fang, H. Liu, and S. Fu, "A compact transmission line self-matched negative group delay microwave circuit," *IEEE Access*, vol. 5, pp. 22836–22843, 2017.

[26] G. Chaudhary, Y. Jeong, and J. Lim, "Miniaturized dual-band negative group delay circuit using dual-plane defected structures," *IEEE Microw. Wireless Compon. Lett.*, vol. 21, no. 1, pp. 19–21, Jan. 2011.

[27] T. Shao, S. Fang, Z. Wang, and H. Liu, "A compact dual-band negative group delay microwave circuit," *Radioengineering*, vol. 27, no. 4, pp. 1070–1076, Dec. 2018.

[28] B. Ravelo, "Methodology of elementary negative group delay active topologies identification," *IET Circuits Devices Syst.*, vol. 7, no. 3, pp. 105–113, May 2013.

[29] B. Ravelo, W. Rahajandraibe, Y. Gan, F. Wan, N. M. Murad, and A. Douyère, "Reconstruction technique of distorted sensor signals with low-pass NGD function," *IEEE Access*, vol. 8, pp. 92182–92195, 2020.

[30] B. Ravelo, "On the low-pass, high-pass, bandpass and stop-band NGD RF passive circuits," *URSI Radio Sci. Bull.*, vol. 2017, no. 363, pp. 10–27, Dec. 2017.

[31] H. Mao, L. Ye, and L.-G. Wang, "High fidelity of electric pulses in normal and anomalous cascaded electronic circuit systems," *Results Phys.*, vol. 13, no. 102348, pp. 1–9, Jun. 2019.

[32] M. T. Abuelma'atti and Z. J. Khalifa, "A new CFOA-based negative group delay cascadable circuit," *Anal. Integr. Circuits Signal Process.*, vol. 95, no. 2, pp. 351–355, May 2018.

[33] Y. Meng, Z. Wang, S. Fang, T. Shao, and H. Liu, "A broadband switchless bi-directional amplifier with negative-group-delay matching circuits," *Electronics*, vol. 7, no. 9, pp. 1–11, Aug. 2018.

[34] F. Wan, L. Wang, Q. Ji, and B. Ravelo, "Canonical transfer function of band-pass NGD circuit," *IET Circuits, Devices Syst.*, vol. 13, no. 2, pp. 125–130, Mar. 2019.

[35] B. Ravelo, F. Wan, J. Nebhen, W. Rahajandraibe, and S. Lalléchère, "Resonance effect reduction with bandpass negative group delay fully passive function," *IEEE Trans. Circuits Syst. II, Exp. Briefs*, vol. 68, no. 7, pp. 2364–2368, Jul. 2021.

ALEXANDRE DOUYÈRE (Member, IEEE) received the Ph.D. degree in electronics and microwaves engineering from the University of la Reunion, Reunion Island, France, in 2008.

Since 2009, he has been an Assistant Professor and currently the Director of the Physics Department, University of la Reunion. He was the scientific responsible of research projects titled XPRIM and FEDER CARERC2. His research interests include wireless power transfer (WPT) and energy harvesting, nonlinear devices, innovative RF measurements, and low-power microwave and millimeter wave conversion circuits. He is a member of the Organizing Committee of the IEEE RADIO Conference and has been a member of IEEE SIGHT Project named ACTION, since 2016.

GEORGE CHAN (Senior Member, IEEE) received the B.Eng. degree (Hons.) in electronic and communication engineering from the City University of Hong Kong and the M.Sc. degree in electronic and information engineering from The Hong Kong Polytechnic University.

He is currently a Senior Product Safety Engineer with ASM Pacific Technology Ltd. He has coauthored several technical publications in international journals and conference proceedings. His research interests include electromagnetic safety, EMC measurement, and EMC management. He is a member of the IEEE EMC Society TC1 on EMC Management. He is also a member of the IEEE International Committee for Electromagnetic Safety (ICES) Standards Coordinating Committee (SCC39) and a TC95 Sub-Committee Member. He is an International Electrotechnical Commission (IEC) Expert and a Committee Member of IEC TC106/PT63184 on Method for the assessment of electric, magnetic, and electromagnetic fields associated with human exposure.

MATHIEU GUERIN (Member, IEEE) received the degree in microelectronics and telecommunications (engineering) from Polytech Marseille, in 2010, and the Ph.D. degree from the University of Aix-Marseille, in 2010. He was a Research Master in integrated circuits design with the University of Aix-Marseille. He worked as a Technical Leader of the Analog and Radio-Frequency Design Team, IDEMIA-StarChip, for a period of five years and designed chips embedded in SIM cards and contactless bank cards with biometric recognition. He joined Aix-Marseille University, as an Assistant Professor, in 2020. He joined the CCSI Team, IM2NP Laboratory. His research interest includes design and synthesis of circuits in digital electronics. He is also working on methods of modeling and characterizing circuits in analog electronics.

YANG LIU was born in Dalian, Liaoning, China, in 1982. He received the B.Sc. degree in technics of control, measurement and instrumentation from the Dalian University of Technology, Dalian, in July 2004, the B.Sc. and M.Sc. degrees in electronic engineering from the University of Pierre and Marie Curie (UPMC), Paris, France, in July 2007 and July 2009, respectively, and the Ph.D. degree from the IRSEEM/ESIGELEC, University of Rouen, France, in October 2012.

FAYU WAN (Member, IEEE) received the Ph.D. degree in electronic engineering from the University of Rouen, Rouen, France, in 2011. From 2011 to 2013, he was a Postdoctoral Fellow with the Electromagnetic Compatibility Laboratory, Missouri University of Science and Technology, Rolla. He is currently a Full Professor with the Nanjing University of Information Science and Technology, Nanjing, China. His current research interests include negative group delay circuits, electrostatic discharge, electromagnetic compatibility, and advanced RF measurement.

SÉBASTIEN LALLÉCHÈRE (Member, IEEE) was born in Nevers, France, in 1979. He received the M.Sc. degree in computational modeling and electronics/electromagnetism from Polytech Clermont, in 2002, and the Ph.D. degree in computational modeling and electronics/electromagnetism from Universite Blaise Pascal, Clermont-Ferrand, France, in 2006.

He worked as a Research Engineer with LASMEA, Clermont-Ferrand, in 2007, focusing on intensive computational methods for electromagnetics. He is currently an Associate Professor with the Institut Pascal and Universite Clermont Auvergne, Clermont-Ferrand. His research interests include electromagnetic compatibility including antennas and propagation, complex and reverberating electromagnetic environments, electromagnetic coupling, computational electromagnetics, stochastic modeling, and sensitivity analysis in electrical engineering.

WENCESLAS RAHAJANDRAIBE (Member, IEEE) received the B.Sc. degree in electrical engineering from Nice Sophia-Antipolis University, France, in 1996, the M.Sc. degree (Hons.) in electrical engineering from the Science Department, University of Montpellier, France, in 1998, and the Ph.D. degree in microelectronics from the University of Montpellier. Since 1998, he has been with the Robotics and Microelectronics Laboratory of Montpellier (LIRMM), Microelectronics Department of Informatics. Since 2003, he has been with the Microelectronics and Nanoscience Laboratory of Provence (IM2NP), Microelectronic Department of Materials, Marseille, France where he was an Associate Professor. Since 2014, he has been a Professor with Aix-Marseille University, where he heads the Integrated Circuit Design Group, IM2NP Laboratory. He is currently a Full Professor with the University of Aix-Marseille. He is regularly involved to participate and to lead national and international research projects (ANR, H2020, and FP7 KIC-InnoEnergy). He directed and co-supervised 18 Ph.D. and 15 master's students. He is the author or coauthor of 11 patents and more than 150 articles published in refereed journals and conferences. His research interests include AMS and RF circuit design from transistor to architectural level. His current research activity is focused on ultralow power circuit design for smart sensor interface and embedded electronic in bioelectronic and e-health applications, wireless systems, design technique, and architecture for multi-standard transceiver. He is an Expert for the ANR, the French Agency for Research. He has served on program committees of IEEE NEWCAS and ICECS. He has been and is a Reviewer of contributions submitted to several IEEE conferences and journals, such as ISCAS, NEWCAS, MWSCAS, ESSCIRC, ESSDERC, RFIC, IEEE Transactions on Circuits and Systems—I: Regular Papers, IEEE Transactions on Circuits and Systems—II: Express Briefs, and *IET Electronics Letters*.

BLAISE RAVELO (Member, IEEE) is currently a University Full Professor with NUIST, Nanjing, China. He is a Lecturer of circuit and system theory, science, technology, engineering and maths (STEM), and applied physics. He is a pioneer of the negative group delay (NGD) concept about t < 0 signal travelling physical space. This extraordinary concept is potentially useful for anticipating and prediction all kind of information. He was a Research Director of 11 Ph.D. students (eight defended), postdoctors, research engineers, and master internships. With U.S., Chinese, Indian, European, and African partners, he is actively involved and contributes on several international research projects (ANR, FUI, FP7, INTERREG, H2020, Euripides[2], and Eurostars). His research interests include multiphysics and electronics engineering. He is a member of *IET Electronics Letters* Editorial Board as a Circuit and System Subject Editor. Since 2013, he has been a member of the Scientific Technical Committee of Advanced Electromagnetic Symposium (AES). He is ranked in Top 2% world's scientists based on years 2019 by Stanford University, USA with Google Scholar H-index(2021)=22 and i10-index(2021)=64. He is a member of research groups: IEEE, URSI, GDR Ondes, Radio Society, and (co)authors of more than 350 scientific research articles in new technologies published in international conference and journals. He is regularly invited to review articles submitted for publication to international journals, such as IEEE Transactions on Microwave Theory and Techniques, IEEE Transactions on Circuits and Systems—I: Regular Papers, IEEE Transactions on Electromagnetic Compatibility, IEEE Transactions on Industrial Electronics, IEEE Access, *IET CDS*, and *IET MAP*, and books (Wiley and Intech Science).

• • •